RSC Advances

ROYAL SOCIETY OF CHEMISTRY

www.rsc.org/advances

Poor solvent and thermal annealing induced ordered crystallites in poly(3-dodecylthiophene) films

I. Roy and S. Hazra*

Influence of poor solvent and thermal annealing, with their definite roles, on the crystalline ordering of poly(3-dodecylthiophene) [P3DDT] films, which is of immense importance in their performance as semiconducting materials, were investigated using complementary techniques. *Edge-on* oriented crystallites (of Form-II like) are enhanced in the as-cast films prepared after addition of the poor solvent. However, the coil-to-rod-like conformational transition is found even more compared to the crystallites, suggesting poor solvent predominantly helps to overcome the unfavorable conformational transition. Huge enhancement of the crystallites (of Form-I like) is observed for the film annealed above the melting temperature of the alkyl side chains, suggesting thermal annealing essentially helps the diffusion of rod-like chains and to overcome the hindrance of the π-π stacking. Perfectly *edge-on* oriented crystallites, which are enhanced with annealing temperature, starts to deteriorate when the melting temperature of the polymer backbone sets in. Domain-like morphology of the as-cast film, however, remains almost unchanged upon thermal annealing suggesting spontaneous organization of π-stacked layers through alkyl side chains to form crystallites is essentially within the small domains. Best *edge-on* oriented crystallites are found for the P3DDT films prepared from solution containing large amount of poor solvent and subsequently annealing the film at around 130°C.

1 Introduction

In the recent years semiconducting polymers are being widely used for the fabrication of organic electronic devices like organic light-emitting diodes (OLEDs),[1,2] polymer solar cells (PSCs)[3,4] and thin film transistors (TFTs).[5,6] In this regard poly(3-alkylthiophenes) (P3ATs), belonging to the large class of π-conjugated polymers, have gained extreme importance due to their availability, easy processing techniques and high charge carrier mobility.[5,7,8] Their high conjugation length endows them with high charge carrier mobility, whereas the flexible long alkyl side chains attached to their stiff backbones makes them easily soluble in common organic solvents,[9,10] which is why they are suitable for the fabrication of photovoltaic devices using simple solution processing techniques.[11] The chemical incompatibility between the π-conjugated polythiophene backbone and the alkyl side chains gives rise to a lamellar structure (as shown in Fig. 1) containing alternate layers of polythiophene backbone and alkyl chains.[12] The semicrystalline nature of P3AT results from the presence of such lamellar regions along with amorphous interlamellar regions. The lamellae can adopt two possible orientations on a substrate - the *edge-on* and the *face-on* orientations. The orientation and ordering in P3AT films greatly influence their performance as semiconducting materials as the field-effect mobility of devices strongly depend on them. The orientation and order can be influenced by various factors such as regioregularity and molecular weight,[7,13] length of alkyl side chain,[14] the solvent from which the film is cast,[15] nature of the substrate[16] and deposition techniques like drop-casting, spin-coating, dip-coating and directional epitaxial crystallization.[17–20]

Saha Institute of Nuclear Physics, 1/AF Bidhannagar, Kolkata 700064, India. E-mail: satyajit.hazra@saha.ac.in

Different approaches have been made to increase the cystallinity and control the morphology and microstructure of P3AT films like optimizing the processing parameters, thermal annealing, solvent vapour treatment, etc.[21] A relatively simple method of preparing 1D aggregates of P3ATs had been proposed by Kiriy et al.[22] This method suggests that by adding a poor solvent one can induce ordered main chain collapse of the P3AT molecules resulting in the formation of 1D aggregates driven by solvophobic interactions. A poor solvent having lower volatility than the main solvent resides within the evolving film for a longer time during solvent evaporation, thus aiding in the growth of ordered aggregates.[23] 2D single crystalline nanosheets of P3HT were prepared by Yu et al. using slow evaporation of a diluted mixture of solvents.[24] It was shown that the ratio of the good-to-poor solvents can control the size of the nanostructures. Later on, Chang et al. showed that a high volatility solvent can also lead to enhanced supramolecular assembly if it interacts with the main solvent through hydrogen bonding.[25] However, not much has been studied about poly(3-dodecylthiphene) (P3DDT) which has the longest alkyl side chain among the P3ATs. The longer side chain is responsible for its better solubility, but hinders its crystallizability due to side chain interactions. Because of this reason P3DDT tends to crystallize into spherulites and not nanowhiskers. Xu et al. reported on the successful formation of P3DDT nanowhiskers by the addition of anisole, a poor solvent for P3DDT, to a solution of P3DDT in chlorobenzene or carbon disulfide which are good solvents for the polymer.[26] In this case the crystallites or aggregates were prepared by heating the mixed solution and subsequent cooling and aging the solution, like others. However, no attempt has been made to study the P3DDT films prepared from solutions of different good-to-poor solvent ratio without heating and subsequent an-

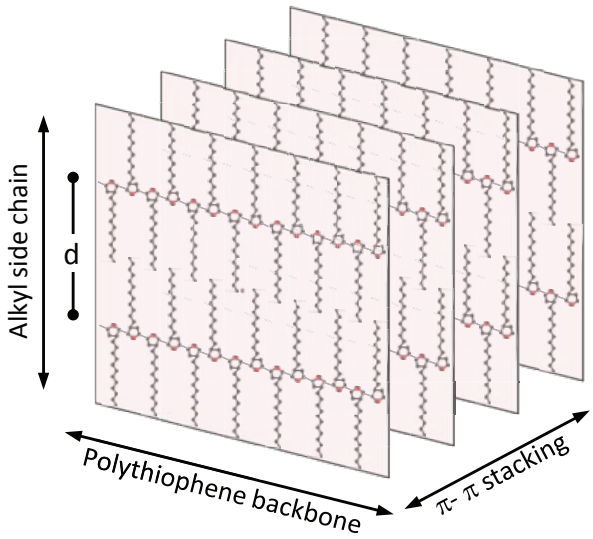

Fig. 1 Schematic of the P3AT crystallite structure, showing π-π stacking, polythiophene backbone (or conjugation) and alkyl side chain directions, and also separation (d) between alternate layers of polythiophene backbones along alkyl side chains.

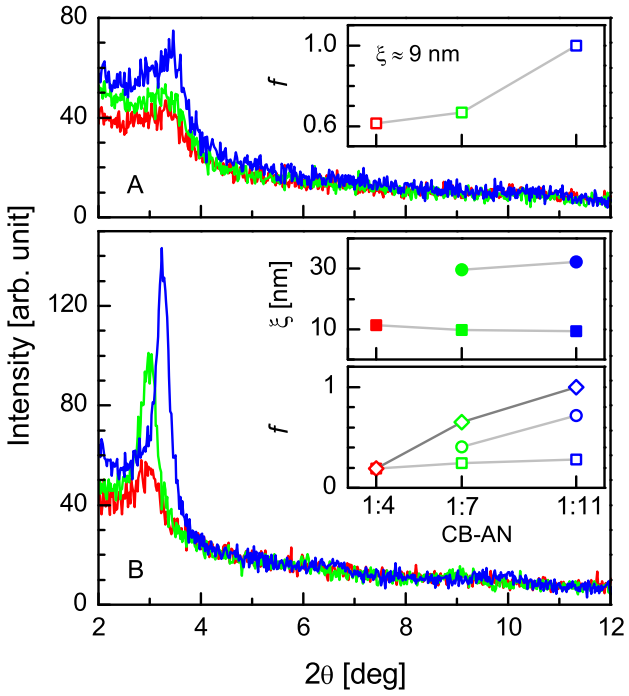

Fig. 2 XRD data (red, green and blue) of the as-cast (A) and 165°C annealed (B) 1:4, 1:7 and 1:11 CB-AN P3DDT films, showing Bragg peak due to the alternate layers of polythiophene backbones and alkyl side chains. Insets: corresponding variation of crystallite size (ξ) and their relative amount (f) with solvent ratio.

nealing of such films at different temperatures to understand the definite role of mixed solvent and annealing temperature on the structures of the P3DDT films. Such understanding will definitely help us to prepare P3DDT films with structures that have possibility to show better device properties.

In this paper, we have exactly tried to understand the role of the poor solvent and annealing temperature on the structures of the P3DDT films, using complementary techniques. For that, P3DDT films, which were first prepared from solutions containing different chlorobenzene-to-anisole ratio without heating and then subsequently annealed at different temperatures, were studied using X-ray diffraction (XRD), grazing incidence X-ray scattering (GISAXS), atomic force microscopy (AFM) and ultraviolet-visible (UV-vis) spectroscopy. Enhancement of rod-like conformation of chains in the films with poor solvent, due to coil-to-rod transition, is clearly evident. Such rod-like chains, which are mostly free or random in the as-cast films, are found to organize to form lamellae or crystallites with thermal annealing. Simple XRD mapping helps us to find the optimum annealing temperature where highly *edge-on* oriented lamellae of maximum amount and/or size are formed, which is of great importance.

2 Experiment

Regioregular poly(3-dodecylthiophene) (P3DDT) was purchased from Sigma-Aldrich (average molecular weight: 60,000; regioregularity $\geq$ 98.5 %) and used as received. Chlorobenzene (CB) and anisole (AN) were obtained from Sigma-Aldrich. P3DDT was first dissolved in CB and then AN was added to that solution such that the concentration of the final solution was 0.25 mg/ml. CB and AN were mixed in the volume ratio 1:4, 1:7 and 1:11. Films were prepared by drop-casting such solutions after about 4 h (as major conversion took place within that time according to the literature,[26] which is also shown in Fig. S1) onto solid substrates and through slow evaporation (by keeping inside petri-dishes). Films deposited on Si substrates from three solutions are referred to as 1:4 CB-AN, 1:7 CB-AN and 1:11 CB-AN. To check the effect of the nature of the Si surface on the film-structure, films were deposited on differently passivated [O- and H-] and oriented [(001) and (111)] Si substrates. O- and H-passivated Si substrates were prepared through pretreatment as reported before.[27–30] To compare the effect of mixed solvent with respect to single CB solvent, films were also prepared on Si substrates from solution of P3DDT in CB solvent. For the optical study, 1:11 CB-AN films were deposited on clean quartz glass substrates. Thermal annealing of the films were done by placing the samples covered in glass petri-dishes in a box furnace. For the annealing at different temperatures, mostly different films were used. For comparison, single 1:11 CB-AN film deposited on glass substrate was also annealed at different temperatures.

XRD measurements of the films were performed on a versatile X-ray diffractometer (VXRD) setup.[31,32] VXRD con-

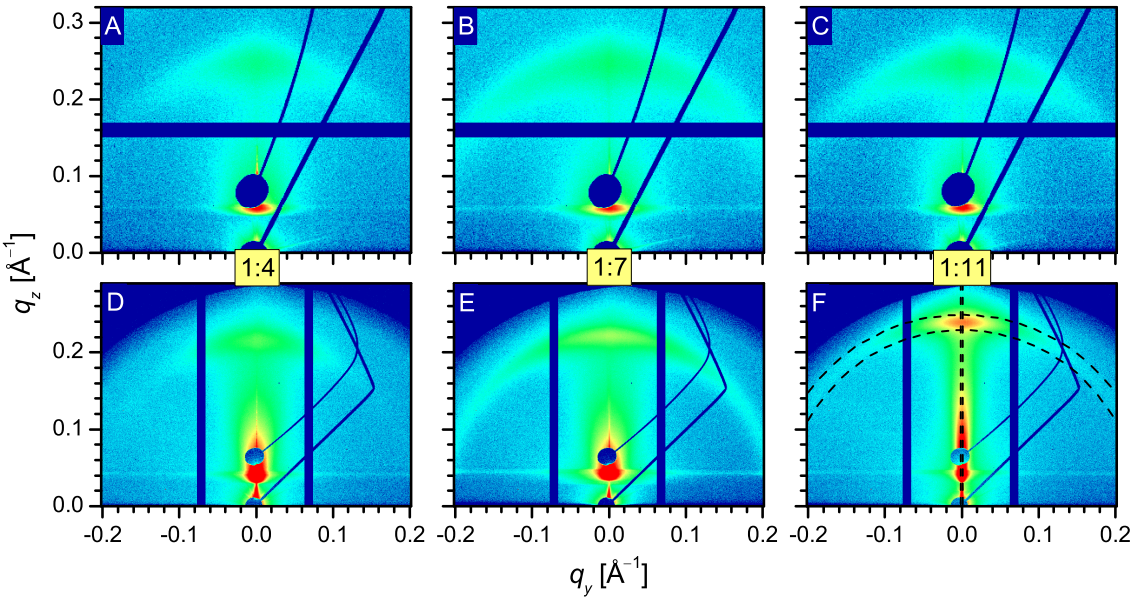

Fig. 3 GISAXS patterns of the as-cast (A, B and C) and 165°C annealed (D, E and F) 1:4, 1:7 and 1:11 CB-AN P3DDT films, showing Bragg arc corresponding to the alternate layers of polythiophene backbones and alkyl side chains.

sists of a diffractometer (D8 Discover, Bruker AXS) with Cu source (sealed tube) followed by a Göbel mirror to select and enhance Cu Kα radiation (λ = 1.54 Å). The diffractometer has a two-circle goniometer $[\theta(\omega) - 2\theta]$ with quarter-circle Eulerian cradle as sample stage. The latter has two circular (χ and ϕ) and three translational (X, Y, and Z) motions. Scattered beam was detected using NaI scintillation (point) detector. Initially, conventional XRD measurements (i.e. $\theta - 2\theta$ scan)[31] were carried out for the as-cast, 60°C and 165°C annealed 1:4 CB-AN, 1:7 CB-AN and 1:11 CB-AN films and also for the films deposited on glass substrates and annealed at different temperatures. Latter rocking (θ) scan[33] around intense Bragg peak ($2\theta_B$) were carried out for one set of mixed solvent (1:11 CB-AN) films and one set of single solvent (CB) films, annealed at different temperatures. Subsequently, XRD measurements for different off-set angle $\Delta\theta$ with respect to the peak position (θ_P) of the rocking curve, were also carried out for those samples. These scans can be used to generate two-dimensional XRD maps.

GISAXS measurements of the as-cast, 60°C and 165°C annealed 1:4 CB-AN, 1:7 CB-AN and 1:11 CB-AN films were carried out using a synchrotron source (P03 beam line, PETRA III)[34–36] at an energy of 13 keV. The scattered beam was detected using a 2D detector (PILATUS 300k, Dectris, having 487 × 619 pixels of pixel size 172 μm). The sample-to-detector distance for the as-cast and annealed samples was 1005 and 1721 mm, respectively. For data collection, the incident angle α was kept at 0.4° and 0.25° for the as-cast and annealed samples, respectively. The direct beam was stopped and the specular reflected beam was attenuated by two separate point-like beam stops to avoid the saturation of the detector.

The top surface morphology of the as-cast, 130°C and 165°C annealed 1:11 CB-AN P3DDT films on Si substrates were mapped through AFM (beam deflection AFM, Omicron NanoTechnology)[29,32] in different length scales (0.2−7 μm). AFM images were collected in noncontact mode and in UHV ($\sim 10^{-10}$ mbar) conditions. Optical absorption spectra of the 1:11 CB-AN P3DDT films on quartz substrates, after annealing at different temperatures, were collected using an UV-vis spectrophotometer (Perkin Elmer, Lambda 750). For comparison, UV-vis spectra of P3DDT solutions, prepared using single (CB) and mixed (CB-AN) solvents, were also collected. For the estimation of the size and/or conformation/structure of P3DDT molecules/aggregates, dynamic light scattering (DLS) measurements (Zetasizer Nano-S, Malvern Instrument) were performed for such solutions.

3 Results and discussion

3.1 Structure from X-ray diffraction

3.1.1 Influence of poor solvent and optimization

In this section, influence of poor solvent on the structures (i.e. amount, size and orientation of the crystallites) of P3DDT films without and with thermal annealing, as observed from the conventional XRD and GISAXS measurements, will be presented to find out the best good-to-poor solvent ratio. Thermal annealing were carried out at 60 and 165°C, which are above two endothermic peaks, observed from DSC thermo-

Table 1 Parameters such as d-value, size (ξ) and normalized amount (f) of the P3DDT crystallites in the as-cast and annealed films prepared from different ratio of good to poor solvents.

Sample	As-cast			165°C annealed					
	d-value (nm)	ξ (nm)	f	d-value (nm)	ξ_1 (nm)	ξ_2 (nm)	f_1	f_2	f
1:4 CB-AN	2.66	9	0.6	2.98	11	-	0.2	-	0.2
1:7 CB-AN	2.66	9	0.7	2.96	10	30	0.2	0.4	0.6
1:11 CB-AN	2.65	9	1.0	2.72	9	32	0.3	0.7	1.0

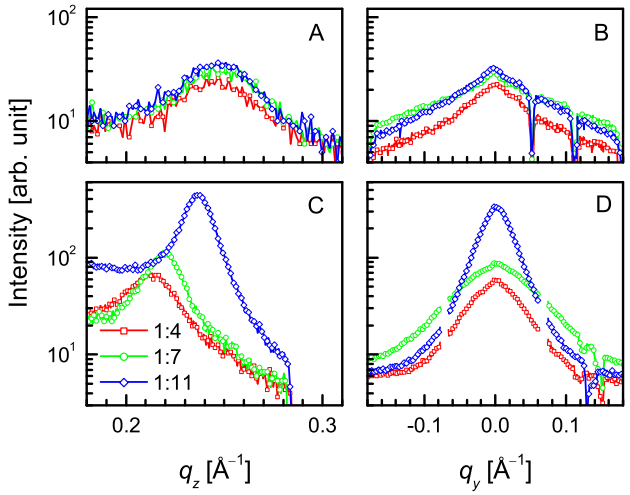

Fig. 4 GISAXS line profiles along q_z (i.e. vertical cut through Bragg spot) and q_y (i.e. horizontal arc through Bragg spot) of the as-cast (A and B) and 165°C annealed (C and D) 1:4, 1:7 and 1:11 CB-AN P3DDT films.

gram of P3DDT powder (shown in Fig. S2), corresponding to the melting of the alkyl side chains and polythiophene backbones, respectively.[37,38]

XRD data of the 1:4, 1:7 and 1:11 CB-AN samples are shown in Fig. 2. Peak around 3.3°, corresponding to the separation (d) between alternate layers of polythiophene backbones along alkyl side chains (as shown in Fig. 1) is observed in all the curves, indicating the presence of small crystallites of P3DDT molecules with predominantly *edge-on* orientations. The position, width and intensity of such peak, however, varies, indicating change in the d-spacing, size and amount of crystallites. For the as-cast films the position is almost same but the intensity increases slightly with the increase in the proportion of the poor solvent. On annealing the films at 60°C there is almost no change (apart from very slight decrease in the position of the peak) in the XRD curves (not shown here). Annealing the films at 165°C results in a huge increase in the peak-intensity and a slight decrease in the peak-position. For the 1:11 CB-AN sample, the change in the intensity is maximum, while that in the position is minimum. Similar nature of XRD patterns (see Fig. S3 of supporting information) is observed for the films deposited on the Si substrates with different passivations and orientations [such as O-Si(111), H-Si(111) or H-Si(001)] and thus needs no separate discussion.

To get the quantitative information about the crystalinity of the films, each XRD data around the peak is fitted with a single or double Gaussian peak(s) along with an exponentially decreasing background. Bragg peak for the as-cast films and the 165°C annealed 1:4 CB-AN film is well fitted with a single Gaussian peak, while that for the 165°C annealed 1:7 and 1:11 CB-AN films is fitted with two Gaussian peaks. Width of the Gaussian peak is used to estimate the crystallite size (ξ) using standard Scherrer's formula

$$\xi = \frac{C\lambda}{\beta \cos\theta_B}$$

where C is a dimensionless Scherrer constant which depends on the shape of the crystallites, the (hkl) index of the diffraction peak and the instrumental factor and whose value is taken to be 0.9, λ is the wavelength of the X-ray, β is the full width at half maxima (FWHM in radian) and θ_B is the Bragg angle. The d-values estimated from the XRD peak positions are tabulated in Table 1. The crystallite size and their normalized amount, estimated from the width and intensity of Gaussian peak(s), are plotted in the insets of Fig. 2 and also tabulated in Table 1. It is clear from the figure and the table that for the as-cast films, very small (~9 nm) size crystallites having d-value of 2.66 nm, are formed. The normalized amount of crystallites increases with the proportion of poor solvent from 0.6 to 1.0. For the 165°C annealed films the crystallites size and/or its amount increases appreciably with the proportion of poor solvent. Relatively large (~30 nm) size crystallites are also formed for the 1:7 and 1:11 CB-AN films, the amount of which is found to be maximum for the latter. The d-value is also found to increase with thermal annealing, the change is minimum for the 1:11 CB-AN films.

GISAXS patterns of the as-cast and 165°C annealed films are shown in Fig. 3. Presence of Bragg arc corresponding to the separation between alternate layers of polythiophene backbones along alkyl side chains is clearly visible in all the patterns. The arc nature suggests that the predominantly *edge-on* oriented lamellae have some deviations as well. There is very little variation in the GISAXS patterns of the as-cast films. The nature remains almost same for the 60°C annealed films (not shown here), while for the 165°C annealed films

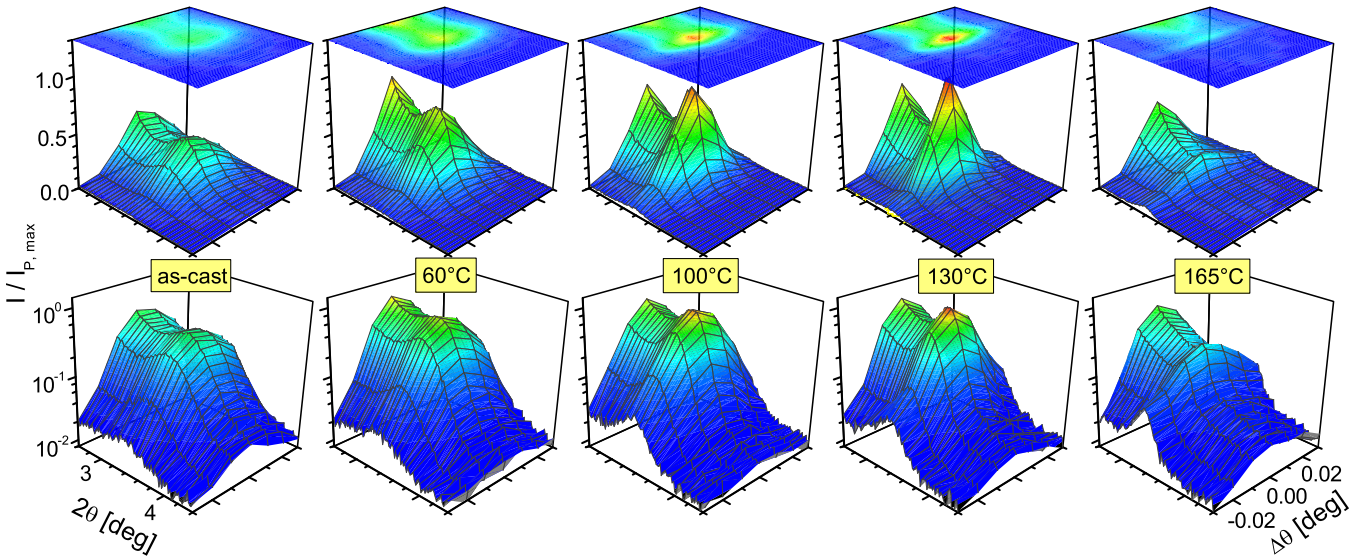

Fig. 5 XRD maps of the as-cast and different temperature annealed 1:11 CB-AN P3DDT films, showing evolution of Bragg peak, corresponding to the alternate layers of polythiophene backbones and alkyl side chains, in three modes of presentation.

the Bragg arc intensity increases, which is small for 1:4 CB-AN film but large for 1:11 CB-AN film. To have a better idea about the film structure, GISAXS line profiles along q_z and q_y directions are generated from vertical cut and horizontal arc, respectively, through the Bragg spot (as shown in Fig. 3) and are plotted in Fig. 4. The GISAXS line profiles along q_z direction (Fig. 4 A and C) exactly follow the XRD data (Fig. 2), hence provides same information about the crystallites. The GISAXS line profiles along q_y direction provides additional information about the orientation of the crystallites. Considering Gaussian distribution, the angular spread in the orientation of the crystallites with respect to the perfect *edge-on* orientation is estimated from FWHM. For the as-cast films, the crystallites are found within the angular spread of $\pm 20^\circ$, with slightly enhanced probability within $\pm 5^\circ$. For the 165°C annealed films, the angular spread decreases, which is minimum for the 1:11 CB-AN film. For this film, the crystallites are found within the angular spread of $\pm 12^\circ$, with strongly enhanced probability within $\pm 5^\circ$.

It is clear from both XRD and GISAXS results that there is a huge difference in the crystalinity for the 165°C annealed films, although a very little difference is observed for the as-cast films. Such apparent anomalous behavior can be understood considering well known two step processes, namely coil-to-rod transformation of the polymers and subsequent organization of rods, to form crystallites. The coil-to-rod transformation is enhanced with the increase in the proportion of poor solvent, while the subsequent organization of the rods to form nearly *edge-on* oriented lamellae are enhanced with the increase in the temperature. At room temperature, few rods probably organized to form very few small ($\sim$9 nm) size crystallites, which we could detect. At higher temperatures, the organization enhanced, which tries to increase the amount and size of the crystallites. However, initial number of rods, which act as nuclei, restrict the amount and size of the crystallites. Accordingly, few small ($\sim$11 nm) size crystallites are found in the 1:4 CB-AN annealed film, while many large (about 32 nm) size crystallites are found in the 1:11 CB-AN annealed film.

3.1.2 Influence of annealing temperature and optimization

In this section influence of annealing temperature on the structure (i.e. amount, size and orientation of the crystallites) of the 1:11 CB-AN (optimum mixed solvent) film, as observed from detailed XRD study, will be presented and compared with the single solvent (CB) film to find out the optimum temperature.

XRD maps of the 1:11 CB-AN samples, collected after annealing at different temperatures, are shown in Fig. 5. Strong evolution of Bragg peak, corresponding to the alternate layers of polythiophene backbones and alkyl side chains, is observed with the annealing temperature. The peak-intensity increases with temperature upto 130°C, then decreases. However, the peak-intensity in directions other than the perfect edge-on direction (clearly visible from 3D log scale presentation) increases gradually. To have a better idea about the film structure, XRD profiles along specular ($\Delta\theta \approx 0$) and off-specular ($\Delta\theta \approx 0.03^\circ$) directions and rocking curves (around $2\theta \approx 3.4^\circ$) for the as-cast, 130°C and 165°C annealed mixed solvent samples are plotted in Fig. 6. XRD profiles and rocking curves for the as-cast, 130°C and 165°C annealed single solvent samples are also plotted in Fig. 6 for comparison. Strong difference is observed between mixed and single

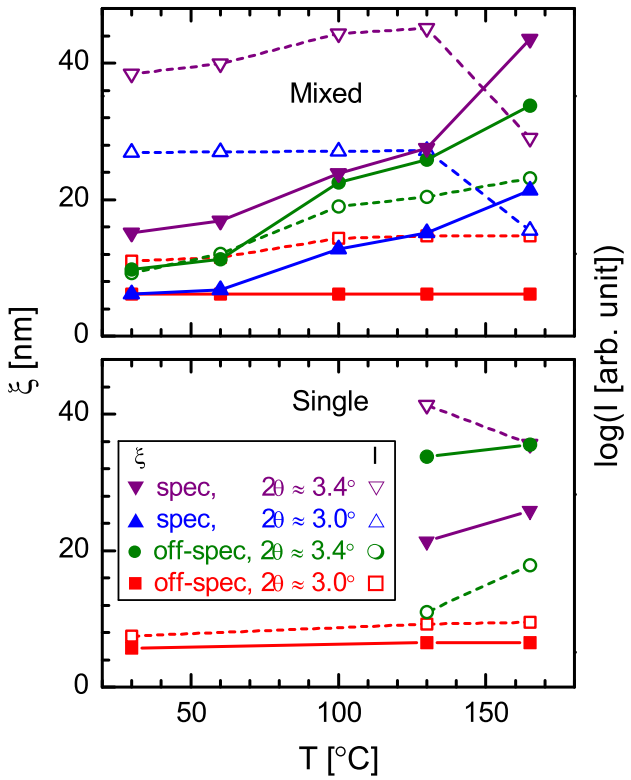

Fig. 7 Variation of the crystallite-size (ξ) and its intensity (I) with annealing temperature along specular and off-specular directions for the mixed and single solvent films.

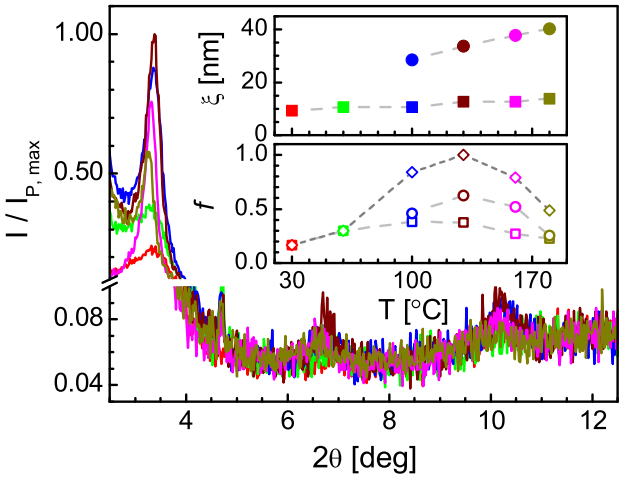

Fig. 8 XRD curves of a as-cast 1:11 CB-AN P3DDT film on quartz glass and after annealing it at different temperatures, showing evolution of Bragg peak, corresponding to the alternate layers of polythiophene backbones and alkyl side chains. Insets: corresponding variation of crystallite size (ξ) and their relative amount (f) with annealing temperature.

solvent as-cast films. The peaks that are present in the XRD curves for the mixed solvent film, both along specular and off-specular directions are almost absent or broad for the single solvent film. The nature of change in the structure of the film with annealing is similar for both films. However, the amount of change is different. Also, the broad hump is still present around the peak in the single solvent film after annealing.

To get detailed quantitative information about the crystalinity of the films, each XRD curve around the peak is fitted with a single or double Gaussian peak(s) along with an exponentially decreasing background, as before. The variation in the size of the crystallites and its amount with annealing temperature along specular and off-specular directions for the mixed and single solvent films are shown in Fig. 7. The increase in the size of the crystallites with the annealing temperature is clearly visible. For the mixed solvent film, two different size crystallites are observed. Along specular direction, ∼6 and 15 nm size crystallites for the as-cast film increases gradually to ∼20 and 44 nm, respectively, on annealing, while along off-specular direction, ∼6 nm size crystallites for the as-cast film remain almost same in size and ∼10 nm size crystallites increase gradually to ∼34 nm on annealing. The intensity or amount of such nanocrystallites along specular direction, which is quite high initially, further increases (or remains almost same) up to 130°C annealing temperature and then decreases considerably, while that along off-specular direction, which is quite low initially, increases gradually with annealing temperature. It can be noted that the XRD and GISAXS results for the different poor solvent films presented before is somewhat average of the results along specular and off-specular directions, which is well expected. As for the XRD measurements of the different poor solvent films, no special alignments have been made, which is required for the estimation along specular direction. Also for the GISAXS measurements, the Bragg peak at $q_y = 0$ has some non-zero q_x component (as the incident angle is $\leq 0.4^\circ$ and the exit angle is $\geq 1.6^\circ$ for $2\theta_B \approx 2^\circ$). For the as-cast single solvent film, no crystallite is observed initially along specular direction, while very low intensity, very small (∼6 nm) size crystallites are observed along off-specular direction. On annealing the film, about 20-25 nm size crystallites are formed along specular direction, while ∼35 nm size crystallites are formed additionally along off-specular direction. The intensity along specular direction is quite high compared to the off-specular direction. Also the intensity along specular direction is maximum around 130°C, while that along off-specular direction increases gradually, similar to the mixed solvent film. Relatively large size crystallites and its normalized amount along specular and off-specular directions for the as-cast, 130°C and 165°C annealed mixed and single solvent P3DDT films are also tabulated in Table 2.

So far we have used different films, for annealing at different temperatures, to understand the structure. We will now cross check it, for a single film annealed at different temperatures. For that, XRD data of a 1:11 CB-AN film on quartz

Table 2 Parameters such as relatively large size crystallites (ξ) and its normalized amount (f) along specular (s) and off-specular (os) directions for the as-cast, 130°C and 165°C annealed mixed solvent (1:11 CB-AN) and single solvent (CB) P3DDT films.

As-cast or annealed at	Mixed solvent film				Single solvent film			
	ξ_s (nm)	f_s	ξ_{os} (nm)	f_{os}	ξ_s (nm)	f_s	ξ_{os} (nm)	f_{os}
As-cast	15	0.4	10	0.2	-	-	-	-
130°C	28	0.9	26	0.5	21	1.0	34	0.3
165°C	44	0.2	34	0.7	26	0.6	36	0.7

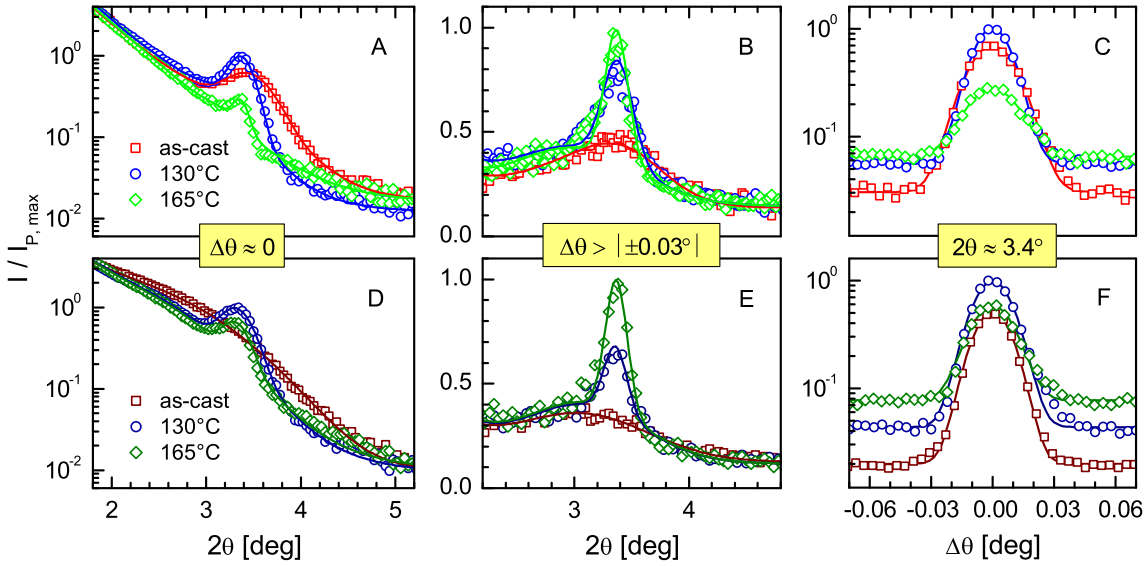

Fig. 6 XRD profiles (along specular, $\Delta\theta \approx 0$ and off-specular, $\Delta\theta \approx 0.03°$ directions) and rocking curves (around $2\theta \approx 3.4°$) for the as-cast, 130°C and 165°C annealed P3DDT films. A, B and C for mixed solvent (1:11 CB-AN) films; D, E and F for single solvent (CB) films.

glass, collected after annealing it at different temperatures, are plotted in Fig. 8. The crystallites size (ξ) and their normalized amount (f), obtained from the peak of each XRD data (as before), are plotted as a function of annealing temperature in the insets of Fig. 8. Considerable increase in the size of the crystallites is observed for annealing above 100°C, the amount of which increases significantly upto 130°C and then decreases, as before. So, XRD analysis of all P3DDT films clearly suggests that the optimum annealing temperature is around 130°C.

3.2 Structure from atomic force microscopy

Typical AFM images of the as-cast, 130°C and 165°C annealed 1:11 CB-AN P3DDT films, in two length scales, are shown in Fig. 9. Island-like structures of the P3DDT films are evident from large scale (5 μm $\times$ 5 μm) topographic images. The size of islands is found in the range of 0.6-0.8 μm, which remains almost unaffected on annealing. The height of the islands, which is about 130 nm for the as cast film, decreases gradually to about 100 nm for 130°C and to about 80 nm for 165°C annealed films. The island-like structure is, however, composed of small domain-like structures, which are clearly evident from small scale (0.5 μm $\times$ 0.5 μm) topographic images. The size of the domains is about 50 ± 10 nm for the as-cast film, which increase slightly to about 60 ± 10 nm for the 130°C annealed film and then decreases slightly to about 45 ± 10 nm for the 165°C annealed film. The height of the compact domains can not be resolved from the images, although the maximum height variation (z_m) within the scan size, is found to decrease with annealing temperature.

3.3 Structure from optical spectroscopy

UV-vis absorption spectra of the 1:11 CB-AN films on quartz glasses, collected after annealing at different temperatures, are shown in Fig. 10. Four shoulders/peaks at about 490, 530, 560 and 610 nm are visible in all the curves. The appearance of well-resolved peaks are mainly due to π-π stacking. The absorption peak around 610 nm originates from the interchain π-π transition, while the absorption peaks at 560, 530 and 490 nm are attributed to 0-0, 0-1 and 0-2 transitions of the intrachain exciton.[39] The peak at about 490 nm can also appear due to intrachain π-π transition from planar rod-like conformation

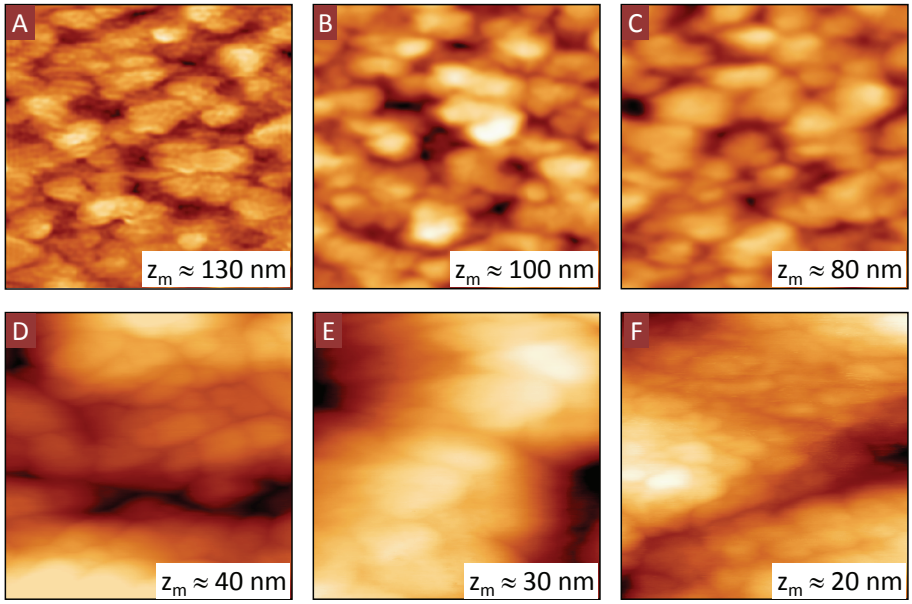

Fig. 9 Typical AFM images in two length scales (A, B and C for scan size: 5 μm $\times$ 5 μm and D, E and F for scan size: 0.5 μm $\times$ 0.5 μm) showing topography of the as-cast (A and D), 130°C (B and E) and 165°C (C and F) annealed 1:11 CB-AN P3DDT films. z_m indicates maximum height variation.

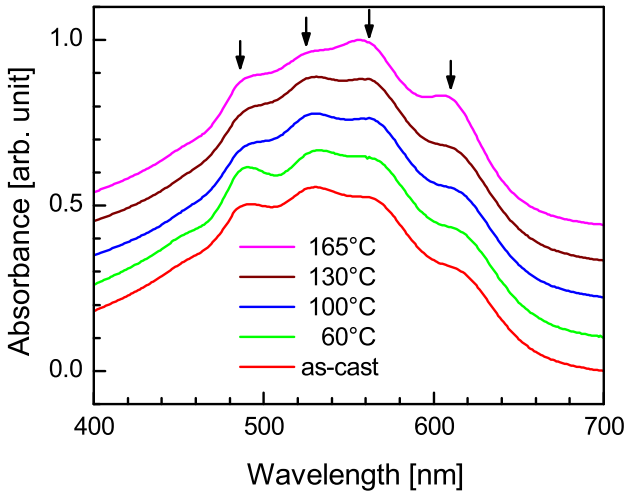

Fig. 10 UV-vis spectra of the as-cast and different temperature annealed 1:11 CB-AN P3DDT films on glass substrates. Peak positions are indicated by arrows.

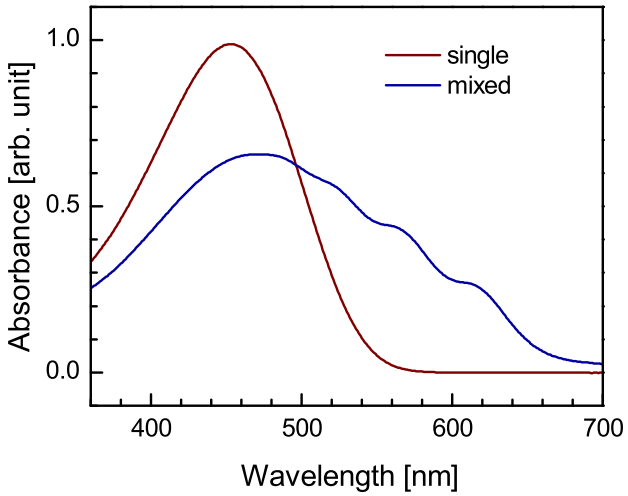

Fig. 11 UV-vis spectra for the solutions of P3DDT in single (good) and mixed (good-to-poor) solvents, collected after 4 h of mixing.

of P3AT chains, which is at about 450 nm for the coil-like conformation of P3AT chains comprising twisting and bending of thiophene rings. The observed spectral signatures can also be described using weakly interacting H-aggregates, where the intensity ratio (A_1/A_2) of the peaks at 610 and 560 nm can be used to extract the free exciton bandwidth of the aggregates, which is related to the coupling strength and conjugation length.[40]

There is almost no peak near 450 nm indicating the presence of very little amount of coil-like conformation chains in the film. The intense peak at round 490 nm for the as-cast film, indicates presence of non-interacting rod-like conformation chains in large amount. Further increase of that peak for the 60°C annealed film indicates presence of enhanced rod-like chains. The intensity of that peak, however, decreases gradually after annealing above 100°C, suggesting decrease in the amount of free rod-like chains, due to the ordering of

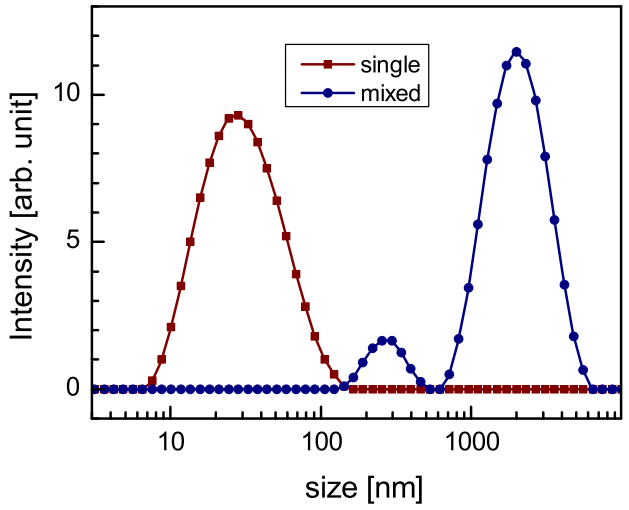

Fig. 12 Intensity particle size distribution curves, obtained from the DLS measurements, for the solutions of P3DDT in single (good) and mixed (good-to-poor) solvents, collected after 4 h of mixing.

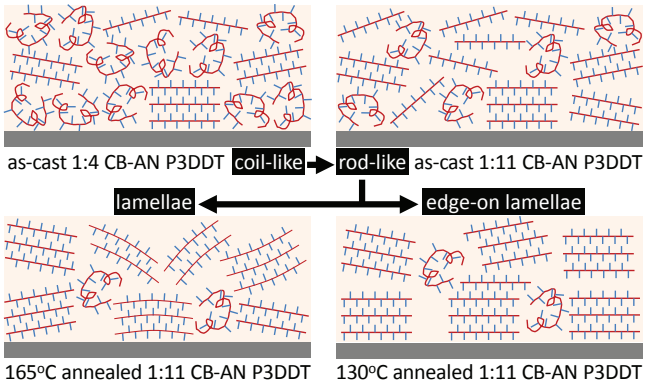

Fig. 13 Schematic illustration of the structures of the P3DDT films showing enhancement of rod-like conformations with poor solvent (for as-cast films), enhancement of lamellae structures (due to subsequent ordering of such rods) with annealing temperature (for 1:11 CB-AN films) and particular enhancement of *edge-on* oriented lamellae near 130°C.

the rod-like chains to form lamellae or H-aggregates, which is evident from the gradual increase in the peak-intensity at around 560 and 610 nm. For the as-cast film and the films annealed upto 130°C, there are very little change in the ratio A_1/A_2, suggesting very little change in the conjugation length. This indicates that the enhancement of lamellae size is predominantly along the alkyl side chain direction. For the film annealed at 165°C, there is a little increase in the ratio and a slight blue shift of the corresponding peaks. Combination of both probably indicates some kind of change in the structure or orientation of the lamellae.

To have better idea about the effect of poor solvent in the structure of P3DDT molecules, UV-vis spectra of the solutions of P3DDT in single (CB) and mixed (CB-AN) solvents, collected after 4 h of mixing, are shown in Fig. 11. Peak near 450 nm is observed in the spectrum of the single solution indicating presence of coil-like conformation molecules, while that peak shifted towards higher wavelength value suggesting presence of predominantly rod-like conformation molecules. Peaks near 530, 560 and 610 nm are also visible in the spectrum of mixed solution, similar to that of the 1:11 CB-AN films, suggesting formation of some P3DDT aggregates in the solution within 4 h.

3.4 Structure from dynamic light scattering

Intensity particle size distribution curves, obtained from the DLS measurements, for the solutions of P3DDT in single (CB) and mixed (CB-AN) solvents, collected after 4 h of mixing, are shown in Fig. 12. Single peak is observed in the curve for the single solution, while two peaks are observed in the curve for the mixed solution. The size obtained from the single solution is about 27 nm, which can be attributed to the average hydrodynamic diameter of the P3DDT, when chains are in coil-like configuration. The size obtained from the mixed solution are about 270 and 2000 nm. The first one can be attributed to the average hydrodynamic diameter of the P3DDT, when chains are in rod-like configuration, while the second one probably corresponds to the size of the aggregates.

3.5 Structures of P3DDT films and growth mechanism

The structures of the P3DDT films deposited from different good-to-poor solvent ratio without thermal annealing (i.e. as-cast) and subsequent annealing at different temperatures, obtained from the analysis of the complementary data, are shown schematically in Fig. 13. In general, the P3DDT films are composed of coil-like and rod-like chains and lamellar crystallites. For the as-cast 1:4 CB-AN film, coil-like chains are more compared to rod-like chains, while for the as-cast 1:11 CB-AN film, rod-like chains are much more compared to coil-like chains. Also few small size lamellar crystallites are present in both the films. For the 60°C annealed film, the amount of rod-like chains increases, while that of coil-like chains decreases. For the films annealed above 100°C, the amount of free rod-like chains also decreases, while the amount and size of the crystallites increases. For the 130°C annealed 1:11 CB-AN film, the amount and/or size of the highly *edge-on* oriented lamellar crystallites are found to be maximum, while for the 165°C annealed film the orientation of the crystallites becomes random.

It is known that P3AT crystallization evolves in two steps, namely, coil-to-rod conformational transition followed by organization of rod-like chains through strong anisotropic π-π interactions between planar rigid backbones and weak van der Waals interactions between their pendent alkyl side chains.[41–43] In a good solvent, P3DDT dissolves well to

form near equilibrium homogeneous system.[26] Such a solution mostly consists of coil-like polymer chains, which are energetically favorable and also clearly evident from both optical absorption and DLS measurements. Addition of a poor solvent makes the solution inhomogeneous and disturbs the equilibrium. Polymers, which are in contact with the poor solvent, experience different polymer-solvent interaction, resulting in a coil-to-rod conformational transition. This is also quite well evident from the optical absorption and DLS measurements.[44] Accordingly, rod conformation increases with the increase of poor solvent. Also aggregates, which are mixed of crystal and amorphous, are formed during this stage (see DLS measurement) and showed up as domains in the film (see AFM images). However, only small amount of rods are organized to form crystallites in the solution and in the as-cast films, prepared after aging and normal drying, which are sensitive to the optical absorption and XRD measurements. This indicates that poor solvent is mainly inducing the unfavorable coil-to-rod conformational transition (negative entropy change) and acting very little on the further unfavorable π-π stacking (which also requires negative entropy change). Thermal annealing seems to be responsible for the π-π stacking. For the present P3DDT polymer, melting of the alkyl side chains takes place in the temperature range 50-80°C, while that of the polythiophene backbones takes place in the temperature range 150-170°C (see Fig. S2). Thus annealing above the first temperature range sets the rod-like polymer chains free and helps the diffusion. Also the thermal energy essentially helps to overcome the unfavorable π-π stacking condition. Increase in the annealing temperature increases the π-π stacking. Organization of the π-π stacked layers through alkyl side chains then initiates to lower the energy. Subsequent cooling predominantly forms *edge-on* oriented crystallites. Room temperature, on the other hand can only induce limited π-π stacking, hence only small crystallites are observed in the as-cast films. Alkyl side chains in such crystallites are slightly interpenetrating and strained (more like Form-II), which on annealing becomes more relaxed (more like Form-I). Annealing the film near the second temperature range twists and deforms the rod-like polymer chains. Such effect increases with the annealing temperature. Accordingly, more deformed and less *edge-on* oriented crystallites are formed on subsequent cooling. It is necessary to mention that the thermal energy not only helps to overcome the unfavorable π-π stacking condition but also to overcome the unfavorable coil-to-rod conformational transition. This is clearly evident for the P3DDT films prepared from single solvent, crystallites of which increases with thermal annealing. However, the thermal annealing along with the initial poor solvent in the mixed solvent films enhanced the overall coil-to-rod conformational transition and the crystallites. Such enhancement with thermal annealing is essentially restricted within small-size domains that are formed in the as-cast film (since not much change in the domain size is observed from AFM).

4 Conclusions

We have shown that P3DDT films with predominantly edge-on oriented lamellae can be prepared by a simple drop-casting method from its solutions in a mixture of a good and a poor solvents, namely, chlorobenzene and anisole; and subsequent thermal annealing of the films. Such lamellae are restricted within small domains (∼50 nm) and nearly isotropic in shape. The degree of crystallinity in the annealed films can be enhanced by increasing the proportion of poor solvent in the solution, as evident from XRD and GISAXS patterns. Annealing beyond the melting temperature of the alkyl side chains and below that of the polythophene backbone brings about an increase in directionality of the lamellae, whereas annealing directly above the melting temperature of the backbone results in increased crystallinity at the cost of decreased directionality, as clearly evident from XRD maps. The XRD data of films cast on hydrophobic H-passivated Si and hydrophilic oxide covered Si show similar nature for both as-cast and annealed films. Similar nature is also observed for films cast on H-passivated Si(001) and Si(111). This means that the P3DDT molecules adopt an edge-on orientation irrespective of the nature of the substrate. Combination of XRD and UV-vis measurements clearly show that rod-to-coil conformational transition is predominently takes place due to the addition of poor solvent in the solution, while organization of the rod-like chains takes place due to subsequent thermal annealing of the film. Annealing beyond the melting temperature of the alkyl side chains helps to form well-ordered *edge-on* oriented P3DDT lamellae structures, which degrades when the melting temperature of polythophene backbone sets in. The optimal annealing temperature for producing well-ordered edge-on oriented P3DDT lamellae turns out to be around 130°C. So the degree of crystallinity and directionality of the semicrystalline polymer P3DDT, which is of immense importance in their performance as semiconducting materials, can be well regulated by varying the good-to-poor solvent ratio and by choosing the proper temperature for post-deposition annealing.

Acknowledgements

The authors thank Dr. S. V. Roth for his support in GISAXS measurements, Prof. P. M. G. Nambissan and Ms. Soma Roy for their help in UV-vis measurements and Prof. M. Mukherjee for providing DLS facility. The financial support received from Saha Institute of Nuclear Physics under DST-DESY project to carry out GISAXS experiments at PETRA III is thankfully acknowledged.

References

1 J. H. Burroughes, D. D. C. Bradley, A. R. Brown, R. N. Marks, K. Mackay, R. H. Friend, P. L. Burns and A. B. Holmes, *Nature*, 1990, **347**, 539.

2 M. Berggren, O. Inganas, G. Gustafsson, J. Rasmusson, M. R. Andersson, T. Hjertberg and O. Wennerstrom, *Nature*, 1994, **372**, 444.

3 G. Yu, J. Gao, J. C. Hummelen, F. Wudi and A. J. Heeger, *Science*, 1995, **270**, 1789.

4 Y. Liang, Z. Xu, J. Xia, S.-T. Tsai, Y. Wu, G. Li, C. Ray and L. Yu, *Adv. Mater.*, 2009, **21**, 1349.

5 L. Qiu, W. H. Lee, X. Wang, J. S. Kim, J. A. Lim, D. Kwak, S. Lee and K. Cho, *Adv. Mater.*, 2009, **21**, 1349.

6 H. Yan, Z. Chen, Y. Zheng, C. Newman, J. R. Quinn, F. Dotz, M. Kastler and A. Facchetti, *Nature*, 2009, **457**, 679.

7 H. Sirringhaus, P. J. Brown, R. H. Friend, M. M. Nielsen, K. Bechgaard, B. M. W. Langeveld-Voss, A. J. H. Spiering, R. A. J. Janssen, E. W. Meijer, P. Herwig and D. M. de Leeuw, *Nature*, 1999, **401**, 685.

8 X. Shen, V. V. Duzhko and T. P. Russell, *Adv. Energy Mater.*, 2013, **3**, 263.

9 K.-Y. Jen, G. G. Miller and R. L. Elsenbaumer, *J. Chem. Soc., Chem. Commun.*, 1986, **17**, 1346.

10 R. Elsenbaumer, K. Jen and R. Oboodi, *Synth. Met.*, 1986, **15**, 169.

11 S. Hotta, S. D. D. V. Rughooputh, A. J. Heeger and F. Wudl, *Macromolecules*, 1987, **20**, 212.

12 S. T. Shabi, E. Mikayelyan, S. Grigorian, U. Pietsch, N. Koenen, U. Scherf, N. Kayunkid and M. Brinkmann, *Macromolecules*, 2012, **45**, 5575–5585.

13 R. J. Kline, M. D. McGehee, E. N. Kadnikova, J. Liu and J. M. J. Frechet, *Adv. Mater.*, 2003, **15**, 1519.

14 V. Causin, C. Marega, A. Marigo, L. Valentini and J. M. Kenny, *Macromolecules*, 2005, **38**, 409.

15 J.-F. Chang, B. Sun, D. W. Breiby, M. M. Nielsen, T. I. Solling, M. Giles, I. McCulloch and H. Sirringhaus, *Chem. Mater.*, 2004, **16**, 4772.

16 R. J. Kline, M. D. McGehee and M. F. Toney, *Nat. Mater.*, 2006, **5**, 222.

17 M. Brinkmann and J.-C. Wittmann, *Adv. Mater.*, 2006, **18**, 860.

18 H. Yang, S. W. LeFevre, C. Y. Ryu and Z. Bao, *Appl. Phys. Lett.*, 2007, **90**, 172116.

19 A. Salleo, R. J. Kline, D. M. DeLongchamp and M. L. Chabinyc, *Adv. Mater.*, 2010, **22**, 3812.

20 S. T. Shabi, S. Grigorian, M. Brinkmann, U. Pietsch, N. Koenen, N. Kayunkid and U. Scherf, *J. Appl. Polym. Sci.*, 2012, **125**, 2335.

21 Y. Fu, C. Lin and F.-Y. Tsai, *Org. Electr.*, 2009, **10**, 883.

22 N. Kiriy, E. Jhne, H.-J. Adler, M. Schneider, A. Kiriy, G. Gorodyska, S. Minko, D. Jehnichen, P. Simon, A. A. Fokin and M. Stamm, *Nano Lett.*, 2003, **3**, 707.

23 Y. D. Park, H. S. Lee, Y. J. Choi, D. Kwak, J. H. Cho, S. Lee and K. Cho, *Adv. Funct. Mater.*, 2009, **19**, 1200.

24 Z. Yu, H. Yan, K. Lu, Y. Zhang and Z. Wei, *RSC Adv.*, 2012, **2**, 338.

25 M. Chang, D. Choi, B. Fu and E. Reichmanis, *ACS Nano*, 2013, **7**, 5402.

26 W. Xu, L. Li, H. Tang, H. Li, X. Zhao and X. Yang, *J. Phys. Chem. B*, 2011, **115**, 6412.

27 H. F. Okorn-Schmidt, *IBM J. Res. Dev.*, 1999, **43**, 351.

28 X. G. Zhang, *Electrochemistry of Silicon and its Oxide*, Kluwer Academic, New York, 2004.

29 J. K. Bal and S. Hazra, *Phys. Rev. B*, 2007, **75**, 205411.

30 P. Chatterjee, S. Hazra and H. Amenitsch, *Soft Matter*, 2012, **8**, 2956.

31 S. Hazra, *Appl. Surf. Sci.*, 2006, **253**, 2154.

32 J. K. Bal and S. Hazra, *Phys. Rev. B*, 2009, **79**, 155405.

33 J. K. Bal and S. Hazra, *Phys. Rev. B*, 2009, **79**, 155412.

34 S. V. Roth, G. Herzog, V. Körstgens, A. Buffet, M. Schwartzkopf, J. Perlich, M. M. A. Kashem, R. Döhrmann, R. Gehrke, A. Rothkirch, K. Stassig, W. Wurth, G. Benecke, C. Li, P. Fratzl, M. Rawolle and P. Müller-Buschbaum, *J. Phys.: Condens. Matter*, 2011, **23**, 254208.

35 P. Chatterjee and S. Hazra, *Soft Matter*, 2013, **9**, 9799.

36 P. Chatterjee and S. Hazra, *J. Phys. Chem. C*, 2014, **118**, 11350.

37 K. Yazawa, Y. Inoue, T. Yamamoto and N. Asakawa, *Phys. Rev. B*, 2006, **74**, 094204.

38 Y. J. Y. Guo and and Z. Su, *Soft Matter*, 2012, **8**, 2907–2914.

39 P. J. Brown, D. S. Thomas, A. Kohler, J. S. Wilson, J.-S. Kim, C. M. Ramsdale, H. Sirringhaus and R. H. Friend, *Phys. Rev. B*, 2003, **67**, 064203.

40 J. Clark, C. Silva, R. H. Friend and F. C. Spano, *Phys. Rev. Lett.*, 2007, **98**, 206406.

41 S. Malik and A. K. Nandi, *J. Polym. Sci. B*, 2002, **40**, 2073.

42 Y. Takizawa, T. Shimomura and T. Miura, *J. Phys. Chem. B*, 2013, **117**, 6282.

43 W. Dierckx, W. D. Oosterbaan, J.-C. Bolsee, W. Maes, D. Vanderzande and J. Manca, *J. Mater. Chem. C*, 2014, **2**, 5730.

44 J. Liu, S. Shao, H. Wang, K. Zhao, L. Xue, X. Gao, Z. Xie and Y. Han, *Organic Electronics*, 2010, **11**, 775.

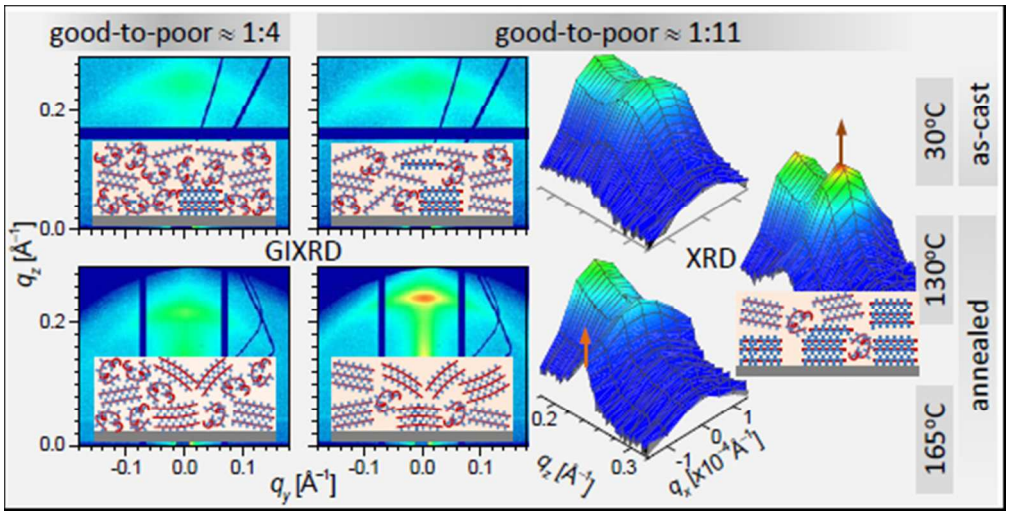

148x75mm (96 x 96 DPI)